Preparation and Properties of Polyethylene–Clay Nanocomposites by an *In Situ* Graft Method

Rongrong Qi, Xing Jin, Chixing Zhou

School of Chemistry and Chemical Engineering, Shanghai Jiao Tong University, Shanghai 200240, China

Received 6 July 2005; accepted 7 June 2006
DOI 10.1002/app.24902
Published online in Wiley InterScience (www.interscience.wiley.com).

ABSTRACT: The polyethylene–clay nanocomposites were prepared by the *in situ* graft copolymerization of styrene containing twin-benzyldimethyldioctadecylammonium bromine modified montmorillonite (TBDO-MMT) in polyethylene with dicumyl peroxide (DCP) as an initiator in molten state. XRD and TEM analysis indicated that intercalated polyethylene/MMT nanocomposites are obtained. The mechanics performance, crystal behavior, thermal properties, and the effect of MMT contents on PE/MMT nanocomposite were also studied. As comparison, polyethylene/montmorillonite composites prepared by a simply melt compounding without styrene were studied as well. © 2006 Wiley Periodicals, Inc. J Appl Polym Sci 102: 4921–4927, 2006

Key words: polyethylene; clay; nanocomposites; graft copolymerization

INTRODUCTION

Layered-silicate-based polymer nanocomposites have recently attracted considerable attention in science and technology because of their significant improvements in mechanical strength and stiffness, gas barrier behavior, thermal, optical, physical–chemical properties, and so on.[1–5] For example, with as little as 2 vol % of montmorillonite (MMT), nylon-6 nanocomposites can possess double of tensile strength and modulus contrasting to the parent polymer.[6,7] In these kinds of nanocomposites, the interfacial effect between the silicate layers and matrix polymers is a key factor, and it can further affect the properties of as-prepared nanocomposites. On the other hand, the dispersion of clay fillers in polymeric matrices also has important effects on the properties of the obtained layered-silicate-based polymer composite. However, the hydrophilic nature of clay does not afford its good dispersion in organic polymer phase, especially in polyolefin, how to improve the interaction between clay and polymer matrix and to produce nanocomposites with good properties has been the pursuit of many scientists.

Polyethylene (PE) is one of the most widely used polyolefin polymers for domestic and industrial applications, and the polyethylene–clay nanocomposites have recently attracted considerable attention. But its compatibility with clay fillers is very poor because it does not contain any polar groups in its backbone, and it is difficult to obtain the nanocomposite in normal ways. To improve the compatibility of clay and polyethylene, the clay is usually modified with alkylammonium groups to facilitate its interaction with a polymer. On the other hand, chemical modification of polyolefin resins with a polar monomer,[8,9] in particular the grafting of pendant anhydride groups,[10–14] has become the main way to enhance its miscibility with inorganic clay, and to prepare polyolefin/clay nanocomposites. For example, Wang et al.[12] have prepared maleated polyethylene/clay nanocomposites in exfoliation and intercalation structure by simple melt process, and they found that the preprepared maleated polyethylene, served as a compatibilitizer, was necessary, and the exfoliation and intercalation behaviors of the obtained nanocomposites were dependent on the amount of maleated polyethylene and the chain length of organic modifier in the clay.

In general, the clay/polymer nanocomposites can be mainly prepared by three methods: solution intercalation, *in situ* intercalative polymerization, and polymer melt intercalation.[2] Among these methods, polymer melt intercalation has proven to be one of the excellent techniques for thermoplastic polymers because of its versatility, compatibility with current polymer processing techniques, and its environmentally benign character due to the absence of solvents.[15] In our previous works, we find that twin-benzyldimethyldioctadecylammonium bromine functionalized montmorillonite (TBDO-MMT) can be well dispersed and swollen in styrene monomer,

Correspondence to: R. Qi (rrqi@sjtu.edu.cn).
Contract grant sponsor: National Science Foundation of China; contract grant number: 50390090.

and polystyrene can been easily intercalated in organic modification MMT.[16] Based on the above-mentioned studies, the polyethylene/montmorillonite nanocomposites were successfully prepared by an *in situ* graft method. Compared with previous works to prepare polyethylene/montmorillonite nanocomposites, the *in situ* graft method is very simple and not any other compatibilitizers were needed. Furthermore, the graft reaction and intercalation proceed simultaneously in the melt compounding, which is beneficial to industry process. The XRD and TEM indicated that intercalated polyethylene/montmorillonite nanocomposites were successfully prepared. And the mechanics performance, crystal behavior, thermal properties, and the effects of MMT contents on PE/MMT nanocomposites were discussed. As comparison, polyethylene/montmorillonite composites prepared by a simply melt compounding without styrene were also studied.

EXPERIMENTAL

Materials

The organophilic montmorillonite (MMT) was kindly supplied by Huate. The cation exchange capacity was about 85–110 meq/100 g of MMT. In general, the organophilic MMT (TBDO-MMT) was prepared by cation exchange between Na^+ in clay galleries and twin-benzyldimethyldioctadecylammonium bromine (TBDO) cations in aqueous solution. Styrene (Shanghai Chemical Solvent) was purified by distillation under reduced pressure at 30°C. Dicumyl peroxide (DCP) (Shanghai Lingfeng Chemical Solvent Factory) was purified by dissolution in hot ethanol, then filtrated and recrystallized at room temperature. Linear low-density polyethylene (LLDPE) (Dowlex 2035, with melt index 6.0 g/10 min and density 0.919 g/cm^3) was purchased from the Dow Chemical Company.

Preparation of LLDPE/MMT composites

The LLDPE/MMT composites were prepared in the molten state using a HAAKE mixer at 180°C and 50 rpm for 15 min. The desired amount of TBDO-MMT and DCP was first dispersed and swollen in styrene monomer. Then LLDPE and the styrene monomer dispersed with clay and DCP were simultaneously introduced into the mixer after blending. To remove the unreacted styrene and formed polystyrene homopolymer, the obtained product (LLDPE-*g*-st-MMT) was extracted with acetone as solvent for 48 h, and then dried to constant weight in a vacuum oven at 80°C for 24 h. The content of insoluble product is about 90 wt %.

TABLE I
Composition of LLDPE/MMT Composites

Samples	LLDPE (g)	TBDO-MMT (g)	Styrene (g)	DCP (mg)
LLDPE-*g*-st-MMT1	50	0.5	6	7.2
LLDPE-*g*-st-MMT2	50	1.0	6	7.2
LLDPE-*g*-st-MMT3	50	1.5	6	7.2
LLDPE-*g*-st-MMT4	50	2.5	6	7.2
LLDPE-*g*-st-MMT5	50	4	6	7.2
LLDPE-*g*-st-MMT6	50	6	6	7.2
LLDPE-*g*-st-MMTC1	50	2.5	3	3.6
LLDPE-*g*-st-MMTC2	50	2.5	9	10.8
LLDPE-MMT1	50	0.5	0	0
LLDPE-MMT2	50	1	0	0
LLDPE-MMT3	50	1.5	0	0
LLDPE-MMT4	50	2.5	0	0
LLDPE-MMT5	50	4	0	0
LLDPE-MMT6	50	6	0	0

For comparison, LLDPE and TBDO-MMT without styrene and DCP were also mixed in melt state.

The detail composition of LLDPE-*g*-st-MMT and LLDPE-MMT composites was listed in Table I.

Characterization of polyethylene/montmorillonite composites

XRD patterns were obtained using a Philips PW1710 X-ray diffractometer equipped with a Ni-filtered Cu Kα source. The voltage and the current of the X-ray tubes were 40 kV and 100 mA, respectively. The basal spacing of the montmorillonite was estimated from the position of the 001 peak in the XRD pattern.

The microstructure of composites was imaged using a JEM-1200EX transmission electron microscope; the ultra-thin film was cut under cryogenic conditions using a Reichert-Jung Ultra-cut E microtome.

Fourier transform infrared (FTIR) analysis was carried out with a PerkinElmer spectrometer (model PARAGON 1000). Thin film samples of 5–10 μm were formed through hot press by placing PE or its composites pellets between two glass slides.

Properties of polyethylene/montmorillonite composites

Crystallization properties were studied by using a PerkinElmer PYRIS-1 differential scanning calorimeter (DSC). Transition temperatures were calibrated using indium and zinc standards. Samples were heated from room temperature to 180°C at a rate of 10°C/min and held for 10 min to destroy any residual nuclei before cooling at 10°C/min. All DSC measurements were performed under an inert (N_2) atmosphere at a heating rate of 10°C/min, and 3–5 mg samples were cut. The thermal stability analysis was performed using a PerkinElmer TGA7 thermogravi-

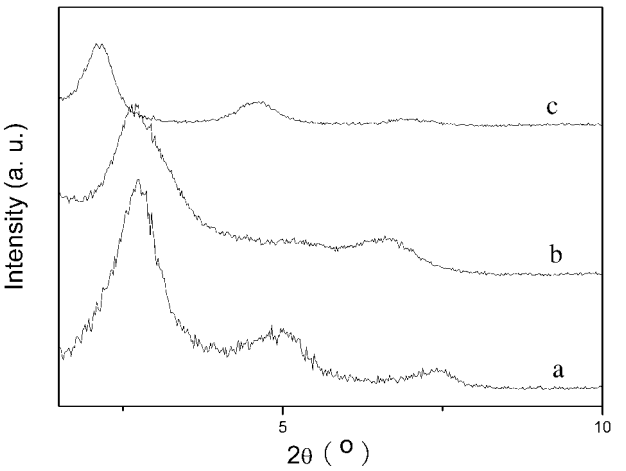

Figure 1 XRD patterns of TBDO-MMT, LLDPE-MMT, and LLDPE-*g*-st-MMT: (a) TBDO-MMT; (b) LLDPE-MMT4 by simple melt compounding; (c) LLDPE-*g*-st-MMT4 by an *in situ* graft method B.

metric analyzer at a heating rate of 20°C/min under nitrogen.

The Izod notch impact strength was measured by Izod instrument (Ray-Ran). All materials were compression-molded in a 2-mm thick plate at 180°C for 5 min. The size of the specimens is 100 mm × 40 mm × 2 mm. The notch was cut by a notch instrument (Ray-Ran).

The different composites were compression-molded (cylinder form: 25 mm diameter, 2 mm height) at 180°C to make samples for measuring the rheological behavior. The rheological properties of each sample were measured by Haake RS600 with a parallel plate geometry using 25 mm diameter plates at 180°C under nitrogen atmosphere. All data were verified in the linear region. The range of frequency in oscillatory shear modes was from 0.01 to 10 rad/s.

RESULTS AND DISCUSSION

Figure 1 shows the XRD patterns of TBDO-MMT, LLDPE-MMT, and PE-*g*-st-MMT. The d_{001} spacing was calculated from Bragg's equation: $d = \lambda/(2 \sin\theta)$, θ is the position of the diffraction peak and λ is 0.1542 nm. As can be seen from Figure 1, the interlayer spacing of the (001) plane (d_{001}) for TBDO-MMT (a), LLDPE-MMT (b), and the LLDPE-*g*-st-MMT (c) is 1.61, 1.63, and 2.08 nm, respectively. Compared the XRD patterns of PE-*g*-st-MMT with TBDO-MMT, the gallery expansion of the (001) plane peak is about 0.47 nm, which indicates that the intercalation structure is obtained by an *in situ* graft method. However, the result is quite different from that when the clay is directly melt-compounded without styrene. Compared the XRD patterns of LLDPE-MMT and that of TBDO-MMT, we can find that the (001) peak of TBDO-MMT does not have any change. This indicates that the intercalation structure of TBDO-MMT and LLDPE cannot be obtained by a simple melt compounding method because TBDO-MMT is immiscible with LLDPE. When styrene was added together with TBDO-MMT, intercalation nanocomposites were obtained which may be because the TBDO-MMT layers were encapsulated by a thin shell of LLDPE-*g*-St, and increased the interlayer distance.[17]

From the above-mentioned results, we can find that the styrene plays a key factor to successfully prepare LLDPE-MMT nanocomposite. To investigate the effects of styrene, different contents of reactive styrene, filled with the same amount of inorganic compound (5 g TBDO-MMT/100 g LLDPE), were used to prepare LLDPE-*g*-st-clay on a HAAKE Mixer (Fig. 2). The results in Figure 2 indicate that the (001) peaks of the obtained composites were notably shifted from 2.73° to 2.44° with the addition of styrene as little as 6 g styrene/100 g LLDPE, and the diffraction (001) of MMT is at 2.12° when 12 g styrene/100 g LLDPE was added. However, when the content of styrene was increased to above 12 g/100 g LLDPE, the d_{001} did not increase. This result indicates that the intercalation capability has a certain limit, which is similar to the results reported by Wang et al.[18] and Hu et al.[19]

FTIR can give useful information on chemical changes occurring in the system. The infrared spectra of the TBDO-MMT, pure LLDPE, LLDPE-MMT, and LLDPE-*g*-st-MMT are shown in Figure 3. From the IR spectra, we can find that polyethylene has characteristic peaks at 3000–2800, 1470, and 720 cm^{-1}, and TBDO-MMT has its characteristic peaks at 3620 and 1470 cm^{-1} due to the aliphatic C—H vibrations of

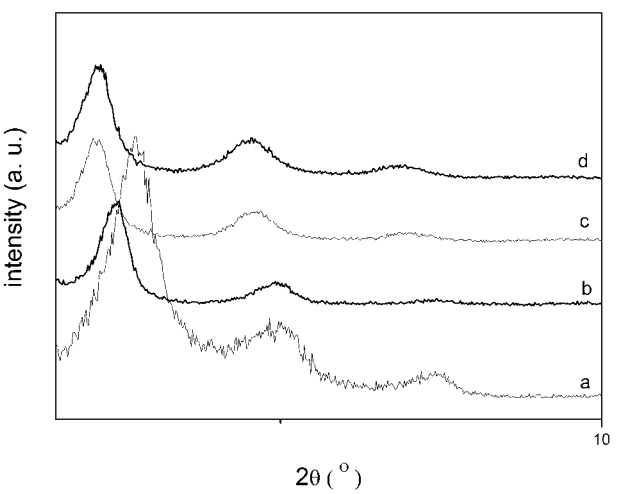

Figure 2 XRD patterns of composites: (a) TBDO-MMT; (b) LLDPE-*g*-st-MMTC1; (c) LLDPE-*g*-st-MMT4; (d) LLDPE-*g*-st-MMTC2.

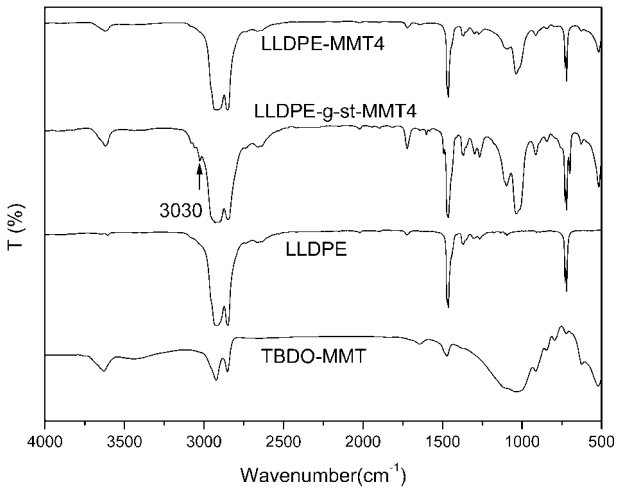

Figure 3 FTIR spectra of TBDO-MMT, LLDPE, LLDPE-*g*-st-MMT, and LLDPE-MMT.

organic modifier aliphatic chains, and 1046 cm^{-1} for Si—O stretching vibrations. Compared to the IR spectra of LLDPE-MMT, the characteristic bands around 3030 cm^{-1} associated with the stretching vibration of C—H in the aromatic ring are observed in LLDPE-*g*-st-MMT, which indicates that styrene has been grafted onto the backbone of polyethylene. On the other hand, we can also find that peaks of MMT centered at 1046 cm^{-1}, compared with LLDPE-MMT and LLDPE-*g*-st-MMT, are deformed and broadened due to overlapping of MMT in the same regions. From IR spectra, we can also find that no any significant differences, except the stronger intensity for LLDPE-*g*-st-MMT, are detected in the composites with or without styrene.

In most cases, TEM combined with XRD can testify the microstructure of the obtained nanocomposites, and it can directly observe the dispersion of TBDO-MMT in the LLDPE matrix. Figure 4 is the TEM imagines of LLDPE-*g*-st-MMT and LLDPE-MMT composites, in which the dark regions are the layers of MMT. From Figure 4(a) we can find that the distribution of MMT layers in LLDPE-*g*-st-MMT4 composite is generally uniform, and it can form some ordered layered silicate. Further studies can find that the intercalated MMT contains many parallel silicate layers. The obtained LLDPE-*g*-st-MMT4 composite with the above microstructure can be considered as an intercalated nanocomposite, and the intercalated structure is in agreement with that observed by XRD

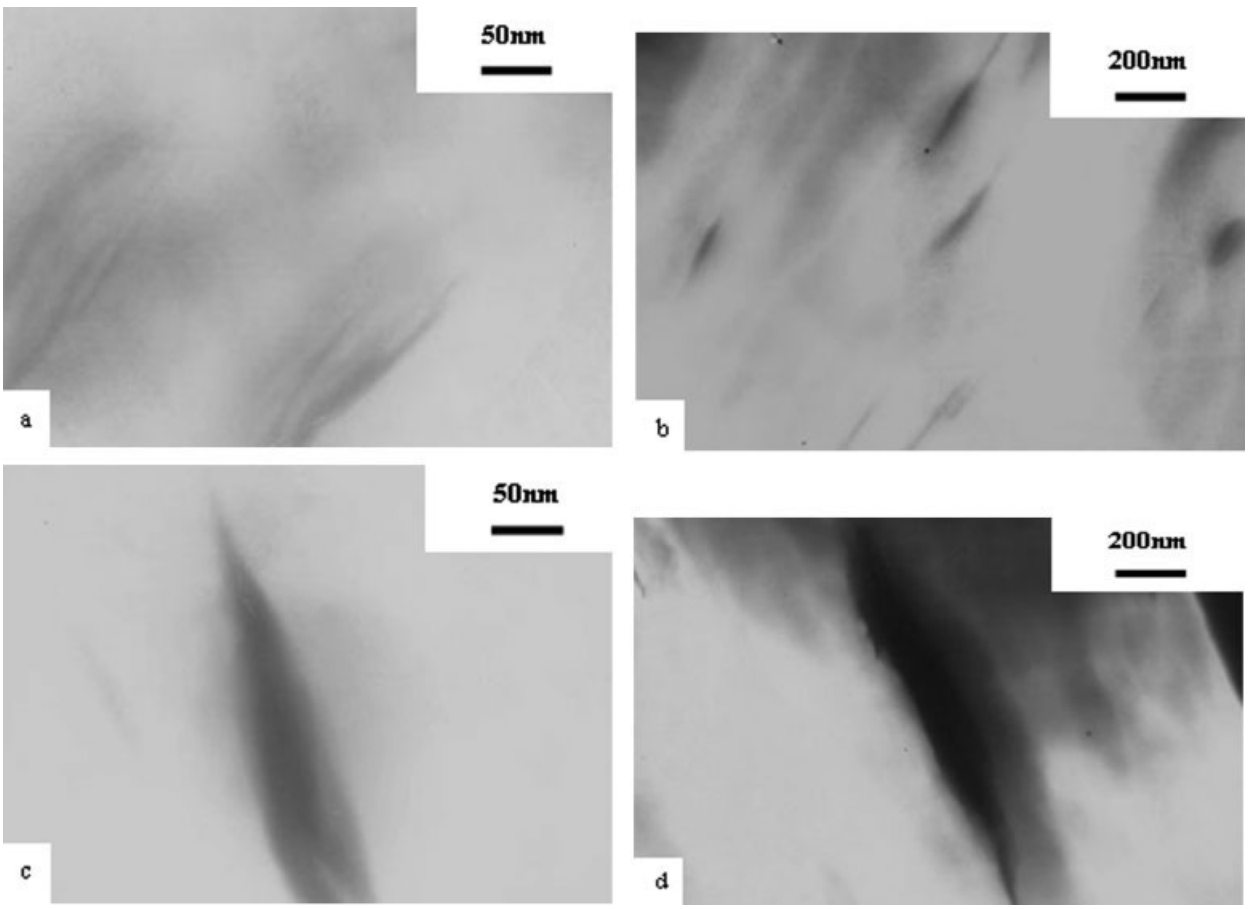

Figure 4 TEM micrographs of PE-MMT composites: (a, b) LLDPE-*g*-st-MMT4; (c, d) LLDPE-MMT4.

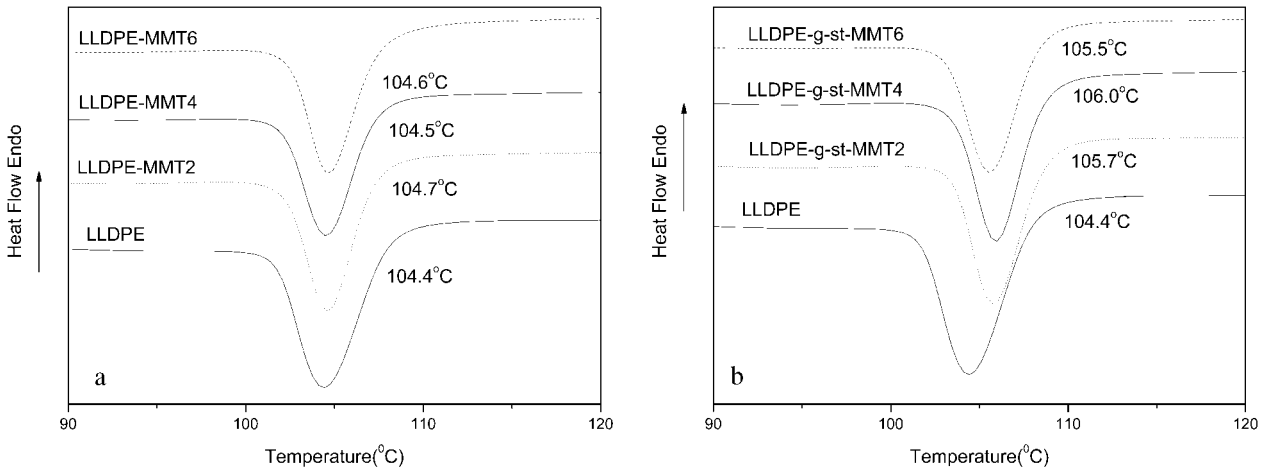

Figure 5 DSC curves of LLDPE/MMT composites: (a) LLDPE-MMT composites; (b) LLDPE-*g*-st-MMT.

shown in Figure 1. As comparison, primary particles composed of many silicate layers can be seen in the LLDPE/MMT composite by simple melt compounding [Fig. 4(c)]. This situation is similar to that of a conventional filled polymer in which primary particles in a few microns are dispersed in the matrix. Compared with Figures 4(b) and 4(d), more homogeneous dispersion of TBDO-MMT is noticed in LLDPE-*g*-st-MMT nanocomposite. The more effective distribution of silicate particles in the nanocomposites may be due to the strong interaction between the styrene and TBDO-MMT. These results indicate that styrene is beneficial to obtain intercalated LLDPE/MMT nanocomposites.

The structural and morphological properties of the LLDPE-*g*-st-MMT nanocomposites have been discussed earlier, and we find that the silicate layers of the LLDPE-*g*-st-MMT nanocomposites were intercalated during graft melt compounding in the presence of styrene. In this case, styrene acts as either the intercalation agent for MMT or as a compatibilizer for the LLDPE and MMT phases.

Because most composites and polymer blends are processed under nonisothermal condition, so to understand the nonisothermal crystallization of LLDPE/MMT composites is of great technological importance. The DSC curves of nonisothermal crystallization for LLDPE, LLDPE/MMT, and LLDPE-*g*-st-MMT composites at a cooling rate of 10°C/min are presented in Figure 5. As seen from this figure, the crystallization temperature (T_c) of LLDPE is 104.4°C, and the additions of TBDO-MMT in LLDPE without the presence of styrene could hardly change the crystallization temperature [Fig. 5(a)]. While the crystallization temperature is up to about 105.7°C when 2 g TBDO-MMT/100 g LLDPE was added into LLDPE together with styrene and DCP, and more addition of clay has a slight influence on the T_c of composites. From the DSC curves of LLDPE/MMT composites, we can also find that the T_c of LLDPE-*g*-st-MMT [shown in Fig. 5(b)] is slightly higher than that of pristine LLDPE because the silicate layers in intercalated LLDPE-*g*-st-MMT would like to act as a nucleating agent for the crystallization. But a smaller temperature shift was observed than the work of Muelhaupt and coworkers.[17] because only intercalated nanocomposites are formed in our work.

To further study the thermal properties of LLDPE-*g*-st-MMT nanocomposites, the TGA curves of LLDPE-MMT and LLDPE-*g*-st-MMT composites are shown in Figure 6. From which, we can find that the decomposition temperatures increase with the adding of TBDO-MMT in the LLDPE-*g*-st-MMT nanocomposites owing to the special intercalated structure of MMT, and the decomposition temperature increases from 470.0 to 486.6°C when 5 g TBDO/100 g LLDPE was added. However, the decomposition temperature decreases with the addition of TBDO-MMT in

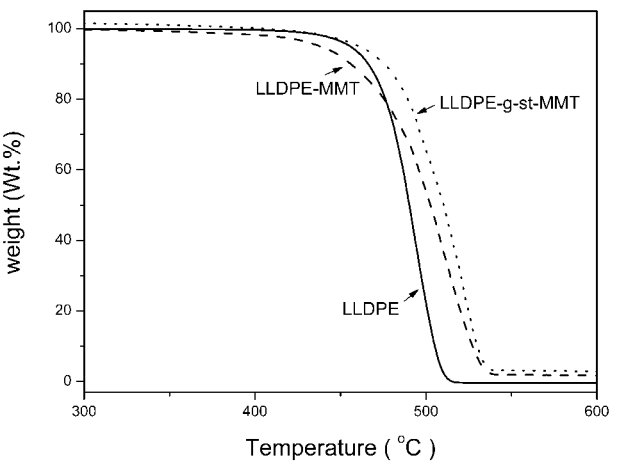

Figure 6 TGA curves of LLDPE/MMT composites.

the simply melt LLDPE-MMT composites because of the poor dispersion of TBDO-MMT in LLDPE matrix.

The amounts of TBDO-MMT also have great effects on the impact strength of LLDPE-MMT composites and LLDPE-*g*-st-MMT nanocomposites (Fig. 7). As to the LLDPE-MMT composites without styrene, the impact strength decreased with the increasing of TBDO-MMT content. This is because the dispersion of TBDO-MMT in LLDPE-MMT composites is poor, and the TBDO-MMT was just like fillers in the normal blending. However, as to the LLDPE-*g*-st-MMT nanocomposites, the impact strength initially increased and then decreased with the increasing of TBDO-MMT, and the maximum value (46.4 kJ/m^2), a 25% increase compared with that of pure LLDPE, was achieved when the concentration of TBDO-MMT was 3 g/100 g LLDPE. The measured mechanical properties truly reflect the effect of intercalation state, and the homogeneous dispersion of MMT clay in polymer matrix leads to improve impact strength. This is because the size of the intercalated interlayers of silicate was in the similar order as that of macromolecular segments, and the increased free volume in the composites made it possible for the segments to move when composites were subjected to an impact force.[9] But at high clay contents, clay particles tend to agglomerate and act as stress concentrators, which may decrease the impact strength. This result is similar to the work of Park et al.[20]

Figure 8 shows the relationship between complex viscosity (η*) and frequency (ω) for LLDPE, LLDPE/MMT, and LLDPE-*g*-MMT. From which, shear thinning pseudonon-Newtonian behaviors are observed, which are similar to those in some conventional thermoplastic composites. Some studies[21,22] on the dispersed flow of particulate-filled polymers demonstrate that the viscosity increases with the filler concentration and, beyond a critical concentration, show a divergence at low frequencies indicating a structural change of the network formed by the particles. The nanometeric dispersion obtained in nanocomposites, together with the high aspect ratio and the shape of the silicate platelets, favors the formation of a structural network already at very low silicate content. It is clear to observe that η* of LLDPE-MMT and LLDPE-*g*-st-MMT increased substantially at low frequencies compared with pure LLDPE, and η* of LLDPE-*g*-st-MMT is the highest, which may be attributed to the particle–particle interactions of good dispersed layered silicate of MMT in LLDPE-*g*-st-MMT and the formation of intercalated structures between LLDPE and MMT.[23,24] With the formation of partial intercalation structures, the interfacial adhesion between MMT and the matrix is dramatically improved and the polymer chain is confined within the silicate layers.[11] It can be supposed that the stronger interfacial interaction and homogeneous dispersion of MMT in LLDPE-*g*-st-MMT and the form of similar flocculated structure lead to higher complex viscosity. This result is similar to that of PBT/clay nanocomposites.[25,26]

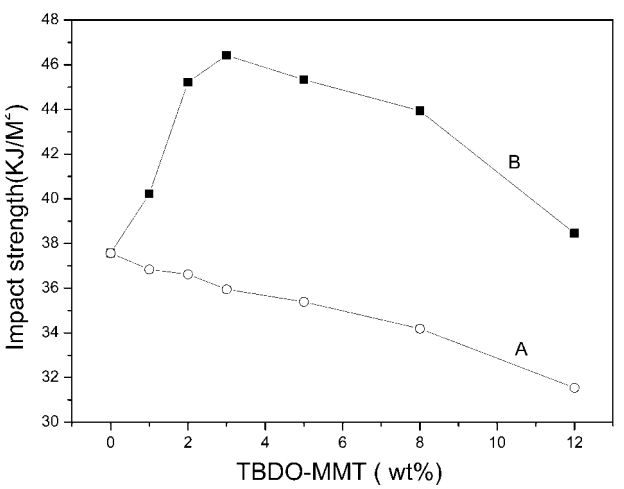

Figure 7 Plots of impact strength versus concentration of TBDO-MMT in (a) LLDPE-MMT composites and (b) LLDPE-*g*-st-MMT nanocomposites.

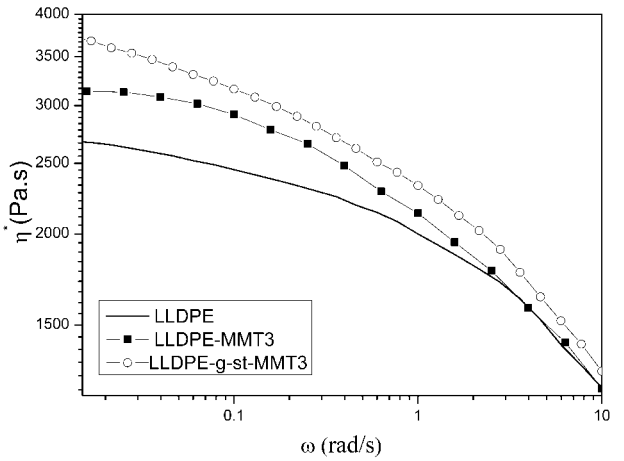

Figure 8 η* versus ω for LLDPE, LLDPE-*g*-st-MMT, and LLDPE-MMT melts.

CONCLUSIONS

The intercalated polyethylene–clay nanocomposites have been successfully prepared by the *in situ* graft copolymerization of styrene containing TBDO-MMT in polyethylene with dicumyl peroxide (DCP) as an initiator in molten state. Compared with the previous works to prepare the polyethylene/montmorillonite nanocomposites, the *in situ* graft method is very simple and not any other polymer compatibilizer is needed because the graft reaction and intercalation proceed simultaneously. Further studies

show that the crystalline temperature, the decomposition temperature and the impact strength of the obtained intercalated LLDPE-*g*-st-MMT nanocomposites have been improved in contrast to the LLDPE-MMT composites and the parent polyethylene.

References

1. Giannelis, E. P. Adv Mater 1996, 8, 29.
2. Alexandre, M.; Dubois, P. Mater Sci Eng R Rep 2000, 8, 1.
3. LeBaron, P. C.; Wang, Z.; Pinnavaia, T. J Appl Clay Sci 1999, 15, 11.
4. Fornes, T. D.; Paul, D. R. Polymer 2003, 44, 3945.
5. Tjong, S. C.; Meng, Y. Z. J Polym Sci, Part B: Polym Phys 2003, 41, 2332.
6. Usuki, A.; Kawasumi, M.; Kojima, Y.; Okada, A.; Kurauchi, T.; Kamigaito, O. J Mater Res 1993, 8, 1179.
7. Yano, K.; Usuki, A.; Kurauchi, T. J Polym Phys Sci, Part A: Polym Chem 1993, 31, 983.
8. Gopakumar, T. G.; Lee, J. A.; Kontopoulou, M.; Parent, J. S. Polymer 2002, 43, 5483.
9. Liang, G. D.; Xu, J. T.; Bao, S.P.; Xu, W.B. J Appl Polym Sci 2004, 91, 3974.
10. Hambir, S.; Bulakh, N.; Kodgire, P.; Kalaonkar, R.; Jog, J. P. J Polym Sci, Part B: Polym Phys 2001, 39, 446.
11. Galgali, G.; Ramesh, C.; Lele, A. Macromolecules 2001, 34, 852.
12. Wang, K. H.; Choi, M. H.; Koo, C. M.; Choi, Y. S.; Chung, I. J. J Polym Sci, Part B: Polym Phys 2002, 40, 1454.
13. Rong, M. Z.; Zhang, M. Q.; Zheng, Y. X.; Zeng, H. M.; Walter, R.; Friedrich, K. Polymer 2001, 42, 167.
14. Zhai, H. B.; Xu, W. B.; Guo, H. Y.; Zhou, Z. F.; Shen, S. J; Song, Q. S. Euro Polym J 2004, 40, 2539.
15. Li, X. C.; Kang, T. Y.; Cho, W. J.; Lee, J. K.; Ha, C. S. Macromol Rapid Commun 2001, 22, 1306.
16. Qi, R. R.; Jin, X.; Nie, J. H.; Yu, W.; Zhou, C. X. J Appl Polym Sci 2005, 97, 201.
17. Kaempfer, D.; Thomann, R.; Muelhaupt, R. Polymer 2002, 43, 2909.
18. Wang, K. H.; Choi, M. H.; Koo, C. M.; Choi, Y. S.; Chung, I. J Polymer 2001, 42, 9819.
19. Wang, S. F.; Hu, Y.; Tang, Y.; Wang, Z. Z.; Chen, Z. Y.; Fan, W. C. J Appl Polym Sci 2003, 89, 2583.
20. Park, J H; Jana, S C. Polymer 2003, 44 2091.
21. Liu, L.; Qi, Z.; Zhu, X. J Appl Polym Sci 1999, 71, 1133.
22. Incarnato, L.; Scarfato, P.; Scatteia, L.; Acierno, D. Polymer 2004, 45, 3487.
23. Khan, S. A.; Larson, R. G. J Rheology 1987, 31, 207.
24. Faulkner, D. L.; Schmidt, L. R. Polym Eng Sci 1977, 17, 657.
25. Ray, S. S.; Okamoto, K.; Okamoto, M. Macromolecules 2003, 36, 2355.
26. Wu, D. F.; Zhou, C. X.; Yu, W.; Xie, F.; J Polym Sci, Part B: Polym Phys 2005, 43, 2807.